Beyond coffee ring: Anomalous self-assembly in evaporating nanofluid droplet on a sticky biomimetic substrate

Lalit Bansal, Pranjal Seth, Sumita Sahoo, Rabibrata Mukherjee, and Saptarshi Basu

Citation: Appl. Phys. Lett. **113**, 213701 (2018); doi: 10.1063/1.5063605
View online: https://doi.org/10.1063/1.5063605
View Table of Contents: http://aip.scitation.org/toc/apl/113/21
Published by the American Institute of Physics

Beyond coffee ring: Anomalous self-assembly in evaporating nanofluid droplet on a sticky biomimetic substrate

Lalit Bansal,[1,a)] Pranjal Seth,[1,a)] Sumita Sahoo,[2] Rabibrata Mukherjee,[2] and Saptarshi Basu[1,b)]
[1]*Department of Mechanical Engineering, Indian Institute of Science, Bangalore 560012, India*
[2]*Instability and Soft Patterning Laboratory, Department of Chemical Engineering, Indian Institute of Technology Kharagpur, Kharagpur, West Bengal 721302, India*

(Received 28 September 2018; accepted 6 November 2018; published online 20 November 2018)

Evaporation induced self-assembly is of paramount importance in many fields ranging from opto-electronic devices, blood spatter analysis, food industry, and thin film deposition. In this article, we report the evaporative drying of a nanofluid droplet on an inclined biomimetic sticky substrate obtained by soft lithographically replicating the structures of Rose petals on crosslinked Polydimethylsiloxane and demonstrate the influence of substrate inclination on the transitions in morphodynamics of the final deposit patterns. Based on experimental data and agglomeration kinetics, we present three unique morphologies induced by substrate inclination. First, buckling from the side in an upright droplet due to air cavity in the substrate. Second, sedimentation induced side buckling in an inclined droplet. Finally, cavity from the bottom in an inverted droplet. We provide a detailed physical explanation of the transition in the morphologies by exploring the coupling among droplet-substrate orientation, evaporation, internal flow and particle agglomeration. *Published by AIP Publishing.* https://doi.org/10.1063/1.5063605

Investigation of particle self-assembly during evaporation of nanofluid droplets is important, owing to its implications in fundamental research as well as in industrial applications. Some of the potential areas are spray drying,[1,2] photonic crystals,[3–5] DNA microarrays,[6–8] to name a few. Due to enhanced reaction, the droplet framework has also been considered for chemical synthesis.[9,10] Furthermore, Song *et al.*[11] used the sessile drop method to investigate the wetting and spreading dynamics of volcanic ash as it melts on high temperature surfaces inside an operating jet engine. Evaporation characteristics are affected by initial conditions such as droplet configuration, type of substrate and ambient conditions. This affects the internal flow field (capillary,[12] Marangoni[13,14] or buoyancy driven[15]), which in turn affects particle self-assembly thereby modifying the morphology of the final precipitate. Various structures of the fully dried precipitate have been reported such as coffee ring,[12] uniform deposit,[13,14] Mexican hat,[16] buckled with inside cavity,[17] dimple formation,[18] cracked precipitates,[19] etc. In our previous work,[17] we have reported that any evaporating nanoparticle laden droplet on a horizontal hydrophobic substrate undergo buckling at the location of minimum shell thickness (at the apex) leaving behind a cavity if the particle concentration is above a critical value. This has been found to be true for heated[20] and confined[21] droplets as well, albeit for specific conditions. On the other hand, cavity formation from the bottom was previously reported by Pauchard and Couder[22] and Chen and Evans[23] in upright evaporating droplets and by Sadek *et al.*[1,2] in inverted droplets. Chen and Evans[23] and Sadek *et al.*[1] attributed it to the air ingression through the contact line. Thus, although the final morphology of the inverted droplet has been observed in the literature, the mechanism leading to it has not been thoroughly explained.

Furthermore, the problem of evaporative drying becomes more complex and fascinating on an inclined surface, as there is often asymmetry in the drop shape due to finite contact angle hysteresis. Understanding droplet evaporation on inclined substrates is useful in spray applications, where gravity driven droplet deformation can affect the uniformity of the coating.[24,25] While there have been several studies involving the evaporative drying of pure water droplets on an inclined plane,[26–28] studies related to evaporation of a colloidal droplet on an inclined plane are limited to only a few theoretical results.[24–26,29] Additionally, a direct comparison between evaporative drying on a flat surface and on an inclined plane (particularly to highlight the effect of inclination) would be ideal if the drop is stationary and does not slide down, which is often the situation on an inclined surface. In this article, we use a sticky surface, fabricated by replicating the features of Rose petals (which are well known for their sticky hydrophobicity), which allows us to compare evaporative morphodynamics of a static drop on an inclined surface, with that obtained on a flat surface, as there is no motion of the drop. Interestingly, evaporation of a colloidal suspension droplet[30] as well as of pure water[31–37] on sticky surfaces have been quite extensively studied, but in all the cases the substrate was horizontal, and therefore the key role of the sticky surface was to ensure that evaporation was in a constant contact radius (CCR) regime.

In this work, evaporation induced particle self-assembly has been investigated at various substrate inclinations. We experimentally demonstrate that the variation in substrate inclination modifies the morphodynamics of the final precipitate. This is due to the coupling among evaporation dynamics, flow pattern and particle self-assembly, which has not been

[a)]L. Bansal and P. Seth contributed equally to this work.
[b)]Author to whom correspondence should be addressed: sbasu@iisc.ac.in.

investigated yet. The resultant experimental observations are then supported by a simplified theoretical analysis of agglomeration kinetics.

A 3 μl droplet is deployed on a rose petal patterned cross linked Polydimethylsiloxane (PDMS) substrate, created by simple double replication of a natural rose petal [details of the patterning procedure are available in the supplementary material (Fig. S1)].[38] The key strength of the patterning technique is the ability to pattern a thin layer of PDMS with a replica molded layer of PDMS comprising the negative replica of the biological petals, which has been ultraviolet/ozone (UVO) exposed for 30 min. UVO exposure leads to a stiff oxide layer formation on the surface of the Stamp for the second replication step and prevents cohesive bonding[39] and avoids much complex approaches adopted for obtaining a positive replica of biological structures.[40] The substrate consists of conical shaped pillars of base diameter 25 μm and height 5 μm (Fig. 1; inset). The droplet is deployed on the substrate and the effect of substrate inclination (α) on the buckling process is studied. The substrate is positioned at different angles ranging from 0° (upright), 30°, 45°, and 60° to 180° (inverted). Experiments are conducted under ambient conditions of 25 °C and 45% relative humidity and images are acquired using a DSLR camera fitted with a Navitar zoom lens. For the evaporation of dispersion droplets, a silica nanoparticle suspension (Ludox TM40 from Sigma Aldrich; avg. diameter: 22 nm; ζ potential: −30 mV) is used at an initial particle concentration of 40 wt. %. Dispersion is found to be stable in the bulk in the absence of evaporation.

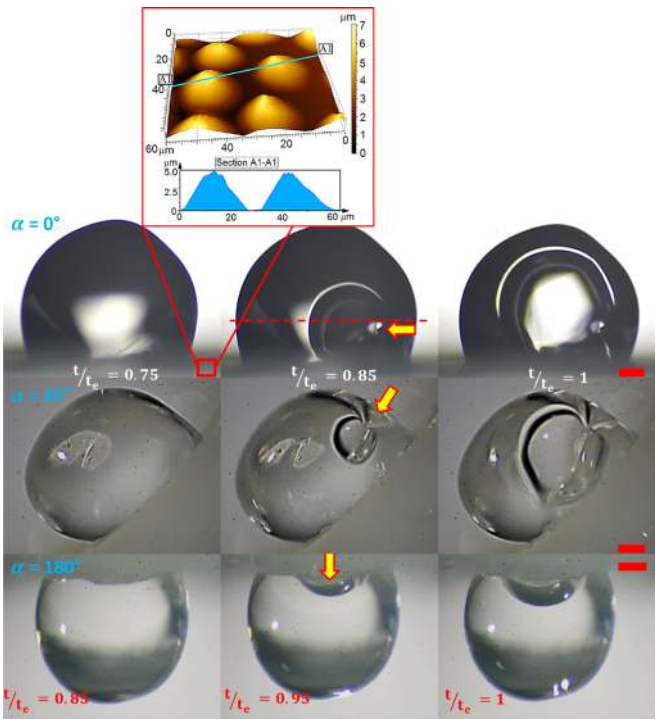

FIG. 1. Snapshots of the evaporating droplet showing cavity growth inside the droplet for different inclinations. Here, t_e denotes the total evaporation time and α denotes the substrate inclination. The dashed red line depicts the upper limit of the buckling location and solid red lines denote the scale bars which equal 200 μm. Arrows depict the location of cavity formation. Normalized timescale at the top (in white) corresponds to the upright (0°) and inclined (45°) cases, while the lower one (in red) corresponds to the inverted droplet (180°). Inset: AFM image of the substrate showing the pillars. Multimedia view: https://doi.org/10.1063/1.5063605.1

For the base case, experiments were first conducted with pure deionized water. It is observed that droplets placed on a rose petal substrate with high adhesion undergo Cassie-Baxter to mixed/impregnated transition in a very short time (Fig. 1, Multimedia view).[41] As a result, the droplet evaporates in a predominantly constant contact radius (CCR) mode with the reduction in the contact radius being only 10%–15% over the droplet lifetime (Fig. S2). Evaporation characteristics are found to be unaffected by the substrate inclination, i.e., the total evaporation time remains within a narrow range (~850 s–900 s) for all the cases. The upright droplet on this substrate assumes an initial contact angle of $\theta_i \sim 134°$, while for that of an inverted droplet $\theta_i \sim 125°$. This 9° decrease is due to stretching of the inverted droplet under gravity. For the inclined cases of 30°, 45°, and 60°, the droplet shape is distorted and thereby two different contact angles are obtained for left ($\theta_{Li} \sim 134°$ for 45° inclination) and right sides ($\theta_{Ri} \sim 116°$ for 45° inclination). This is due to slip of the contact line under the effect of gravity. The increase in the inclination angle increases the difference between the two contact angles: $\Delta\theta = \theta_{Li} - \theta_{Ri}$. The difference gradually becomes zero towards the end of the evaporation lifetime (Fig. S3; angles are normalized by the average of the two contact angles for each droplet).

Next, we investigated the evaporation characteristics of a nanosilica dispersion droplet (initial particle concentration, $\varphi_o =$ 40 wt. %). Figure 1 shows the snapshots of droplet lifetime for selected configurations ($\alpha = 0°$, 45°, and 180°). The upright droplet undergoes buckling as mentioned above (Fig. 1). The only deviation is in the location of buckling onset. Unlike our previous work where buckling is observed from the apex,[17] here the buckling location has shifted close to the contact line although the exact location is random, i.e., it can buckle from anywhere along the droplet periphery below the dashed line (Fig. 1). It is to be noted that in the present work as buckling is always followed by internal cavity growth for upright and inclined droplets, the word "buckling" here loosely refers to buckling induced cavity growth. Similar buckling and subsequent cavity growth are seen even in the case of inclined droplets with the difference that inclined droplets always buckle from the right side (i.e., upper region) of the droplet (Fig. 1). On the other hand, when the droplet is completely inverted, cavity formation is still observed, but it is not because of the buckling instability. The cavity seems to be growing from the substrate (Fig. 1) as explained below. Since an inverted droplet cavity is formed after most of the particles have sedimented (Fig. 2), the cavity growth is initiated slightly later ($\frac{t}{t_e} \approx 0.85$) than that in cases of upright and inclined droplets ($\frac{t}{t_e} \approx 0.75$), and t_e denotes the total droplet evaporation time (Fig. 1).

To understand the mechanism behind the suppression of buckling and cavity growth from the bottom in an inverted droplet, we dispersed 860 nm fluorescent microparticles[42,43] (rhodamine coated polystyrene particles; initial concentration 0.008 vol. %) in the nanosilica suspension. Addition of fluorescent particles serves two purposes; first, the flow field inside the droplet can be visualized, and second, it allows visualization of the growth of sedimentation front. The internal flow field is found to be re-circulatory toroidal in nature. Such a flow field pattern was previously explained by Dash

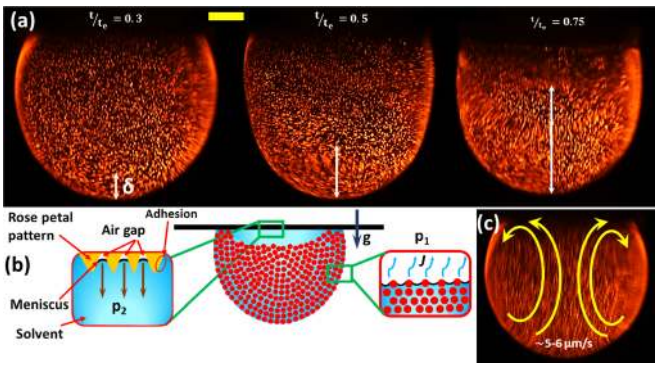

FIG. 2. (a) Images of the inverted droplet showing growth of the sedimentation front (δ) from the apex towards the substrate. Here, t_e denotes the total evaporation time. The image becomes hazy as the sedimentation front grows. White arrows depict the length of agglomeration growth. (b) Schematic showing the mechanism behind cavity formation. Here, p_1 and p_2 are capillary pressures due to evaporation from the droplet periphery and across menisci on the pillared substrate, respectively. (c) Flow field inside the inverted droplet. Scale bar equals 200 μm. Multimedia view: https://doi.org/10.1063/1.5063605.2

et al.[15] and Bansal *et al.*[17] However, in those studies, the flow was buoyancy driven where the flow in the center was directed towards the apex as it was heated up by the substrate. Even in the present work, the temperature near the substrate is greater than the apex owing to evaporative cooling from the droplet periphery. Thus, if buoyancy is the deciding factor, then there would not be any flow due to thermal stratification. Hence, the flow is Marangoni driven, i.e., the decrease in surface tension at the contact line results in a flow towards the apex along the periphery. The flow then returns to the substrate in the center resulting in a toroidal motion [Fig. 2(c), Multimedia view]. As shown in Fig. 2, it is seen that the particles start to sediment from the apex of the droplet and it grows upwards towards the base (δ—length of the sedimentation front). Thus, we can conclude that gravity coupled with evaporation (maximum from apex; height regression rate: 0.6 μm/s) plays a major role in particle sedimentation ($d\delta/dt = 1.9$ μm/s) during inverted droplet evaporation. However, particles can sediment only after they have grown to a critical size. As the particles are circulated by the flow inside the droplet, they collide due to shear and agglomerate as a result of orthokinetic agglomeration. After achieving the critical diameter, agglomerates begin to sediment under gravitational forces.

Bremer *et al.*[44] gave an expression for this critical size at which the agglomerates show significant sedimentation

$$d_c = \left(\frac{3kT}{2\pi a^{3-D}\Delta\rho g}\right)^{1/(D+1)}, \tag{1}$$

where k is Boltzmann's constant, T is the ambient temperature, a is the nanoparticle diameter, and $D = 1.56$ is the fractal dimensionality.[45] From Eq. (1), the value of d_c is found to be ~3.8 μm.

Thus, using this value of d_c, the sedimentation velocity (v_{sed}) can be calculated using the Stokes equation

$$v_{sed} = \frac{g\Delta\rho d_c^2}{18\mu}, \tag{2}$$

where g is the gravitational acceleration, $\Delta\rho = \rho_{particle} - \rho_{water}$, $\rho_{particle}$ and ρ_{water} are the densities of silica nanoparticles and solvent, respectively, and μ is the dynamic viscosity. Theoretical sedimentation velocity obtained is ~3 μm/s. The average flow velocity is found be of the same order of ~3.5–4.5 μm/s (corrected for the lens effect as explained by Kang *et al.*[46] and Dash *et al.*[15]). This implies that the particles will settle at the bottom of the inverted droplet even in the presence of the recirculating flow. Experimental time elapsed between the point of deployment and the point when the sedimentation is first seen is around ~150 s for an inverted droplet. Theoretical time required for the nanoparticles to undergo orthokinetic agglomeration and grow to the size that they may sediment is given by[44]

$$t_c = \frac{\pi D}{4\dot{\gamma}(3-D)}\varphi_o^{-1}\left(1 - \left(\frac{d_c}{a}\right)^{(D-3)}\right), \tag{3}$$

where $\dot{\gamma}$ is the shear rate or velocity gradient. Substituting various values, we get $t_c = 210$ s, which is of the same order as the experimental value of 150 s.

As evaporation continues, water now leaves the droplet through closely packed nanoparticle aggregates (Fig. S4). However, water inside the pillars (due to impregnation) will exit only if the evaporation induced capillary pressure on the periphery is greater than the pressure across the menisci inside the pillars. Evaporation through nanopores induces capillary pressure [Fig. 2(b)], which is given by $p_1 = \frac{\mu\tau J}{\kappa}$, where τ is the sediment thickness, J is the evaporation rate and $\kappa = \frac{1}{180}\frac{(1-p_f)^3}{p_f^2}a^2$ is the permeability; $p_f \sim 0.64$ is the packing fraction (considering close random packing). Here, $\tau \sim 0.1$ mm considering the minimum distance from the periphery to the cavity, which is close to the substrate. On the other hand, the pressure acting across the menisci in the pores is $p_2 = 2\sigma/r_p$ [Fig. 2(b)], where σ is the surface tension and $r_p \approx 6$ μm (considering penetration height is half the pillar height) is the pore radius obtained from AFM image. From the above two equations (p_1 *and* p_2), it is seen that the force corresponding to evaporation controlled capillary pressure ($F_1 \sim 96$ mN) is greater than the force corresponding to pressure across the menisci on the pillared substrate ($F_2 \sim 4$ mN). The third force due to adhesion between water and the substrate is ($F_A \sim 0.0638$ mN[47]), which is negligible compared to the aforementioned pressure forces. Thus, as the water layer is detached from the substrate, air is sucked in from the pores as well as the environment resulting in the formation of a cavity. Once the droplet has completely dried, cracks form breaking the final precipitate into small pieces. Thus, it is difficult to image the bottom cavity in the dried sample. To verify that the air ingression is not just because of the patterned substrate, we repeated the experiment on a smooth PDMS substrate and observed the similar behavior. In the case of PDMS, pressure due to menisci is absent. Thus, only capillary pressure is significant as the adhesion force is negligible. Figure S5 shows the cavity hole at the base of the precipitate dried on the PDMS substrate.

Similar sedimentation is observed for an inclined droplet as shown in Fig. 3. In the case of an inclined droplet,

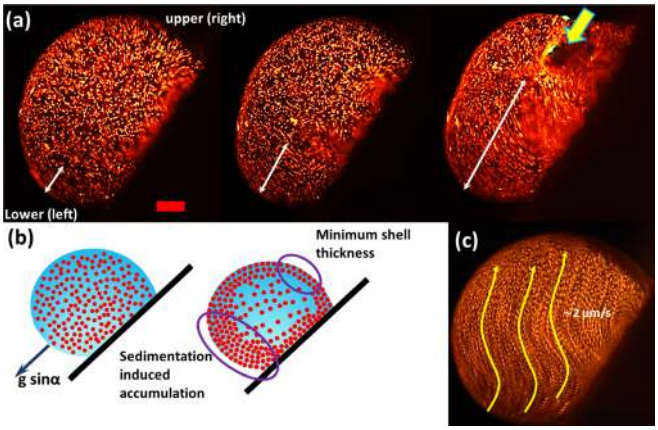

FIG. 3. (a) Fluorescent images of the inclined droplet (at 45°) showing particle accumulation from the apex towards the substrate. White arrows depict the length of agglomeration growth. (b) Schematic showing the mechanism behind buckling from side. (c) Flow field inside the inverted droplet. Scale bar equals 200 μm. Multimedia view: https://doi.org/10.1063/1.5063605.3

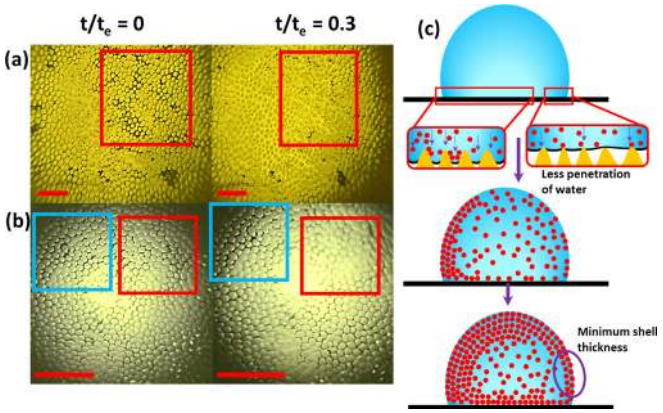

FIG. 4. (a) and (b) Snapshots showing water penetration inside the pillars of the superhydrophobic substrate. Red boxes denote the transition to the impregnated state and blue boxes denote the Cassie Baxter state. (c) Schematic showing the mechanism behind buckling instability leading to cavity formation. Scale bar equals 200 μm. Here, t_e denotes the total evaporation time.

particles sediment on the lower part (left side) of the droplet even though evaporative flux is slightly higher in the upper part (due to low contact angle; Fig. 3). Gravitational force also affects the internal flow field as shown in Fig. 3 and Multimedia view. The competition between the relatively high evaporation flux on the upper part and the gravity on the lower part results in a single toroid flow field. Using similar equations as in the case of the inverted droplet albeit replacing g with $g \sin\alpha$, we get the sedimentation velocity as 2.2 μm/s. This is in corroboration with the average velocity obtained from experimental data; 2 μm/s (corrected value). Furthermore, theoretical time [Eq. (3)] required for sedimentation is also found to be close to its experimental counterpart; $t_{c,theo} = 650$ s and $t_{c,\exp} = 540$ s. As the sedimentation front grows up on the left side of the droplet [Fig. 3(a) and Multimedia view], evaporation continues from the right side maintaining the internal flow field locally (Multimedia view). Thus, the formation of the visco-elastic shell on the right side is delayed. As a result, the location of minimum shell thickness is on the right side of the droplet which subsequently buckles under capillary pressure ($p = \frac{\mu\tau J}{\kappa}$; as defined earlier).[17] Thus, for an inclined droplet, buckling location is observed on the upper part (right side; near the apex). After buckling, the shell ruptures resulting in a cavity inside the droplet.

Finally, we look at the upright droplet evaporating on a rose petal patterned substrate. For this case, sedimentation is weak as the theoretical sedimentation velocity ~3 μm/s is slightly lower than the evaporation induced flow velocity ~5 μm/s which are acting in opposite directions. Thus, unlike an inverted or inclined droplet, there is no noticeable sedimentation inside the upright droplet. Moreover, as mentioned before, buckling location on the current substrate is different from that observed on smooth PDMS substrate.[17] To explain this discrepancy, we hypothesize that it is due to the inability of the nanoparticles to deposit near the base where there is an air cushion. For nanofluid droplets, as reported by Bansal *et al.*,[17] particles first accumulate near the three-phase contact line. This is due to no slip condition near the substrate and particles accumulate due to orthokinetic agglomeration. Then, following the bottom-top approach, a thin shell is obtained near the apex. However, for the pillared substrate, initially the droplet rests on an air cushion, i.e., in Cassie-Baxter state. Water then penetrates into the pores transforming into a mixed/impregnated state; however, it may not penetrate all the pores as shown in Fig. 4. Thus, we think due to the air cushion, particle accumulation (at locations with less/no impregnation) near the base is delayed at certain locations. This results in the shift of the point of minimum shell thickness (consequently, the buckling location) to the side where particle accumulation is delayed (Fig. 4).

In summary, we experimentally demonstrate that the morphodynamics of the final precipitate on an inclined sticky biomimetic substrate depends on the competition between evaporation and sedimentation. We provide a simplified theoretical analysis to corroborate the experimental data. Substrate inclination also modifies the internal flow field from double toroid buoyancy driven (upright) to single toroid (inclined) and back to double toroid albeit Marangoni driven (inverted). Therefore, this study provides a simple technique for varying the location of cavity initiation, which in turn affects the morphology of the final precipitate just by controlling the substrate inclination. The role of viscosity in morphodynamics due to changes in nanoparticle concentration has not been investigated exclusively and can be found elsewhere.[17] However, it is well documented that viscosity affects the droplet evaporation lifetime due to pinning thereby affecting the shell formation dynamics.

See supplementary material for details on materials and methods, evaporation characteristics of a pure water droplet on an inclined substrate, and movie files showing water impregnation and particle deposition on inverted and inclined droplets.

[1]C. Sadek, H. Tabuteau, P. Schuck, Y. Fallourd, N. Pradeau, C. Le Floch-Fouéré, and R. Jeantet, "Shape, shell, and vacuole formation during the drying of a single concentrated whey protein droplet," Langmuir **29**, 15606–15613 (2013).
[2]C. Sadek, L. Pauchard, P. Schuck, Y. Fallourd, N. Pradeau, C. Le Floch-Fouéré, and R. Jeantet, "Mechanical properties of milk protein skin layers

after drying: Understanding the mechanisms of particle formation from whey protein isolate and native phosphocaseinate," Food Hydrocolloids **48**, 8–16 (2015).
[3]Y. Xia, B. Gates, Y. Yin, and Y. Lu, "Monodispersed colloidal spheres: Old materials with new applications," Adv. Mater. **12**, 693–713 (2000).
[4]O. Sato, S. Kubo, and Z.-Z. Gu, "Structural color films with lotus effects, superhydrophilicity, and tunable stop-bands," Acc. Chem. Res. **42**, 1–10 (2009).
[5]C. I. Aguirre, E. Reguera, and A. Stein, "Tunable colors in opals and inverse opal photonic crystals," Adv. Funct. Mater. **20**, 2565–2578 (2010).
[6]M. Schena, D. Shalon, R. W. Davis, and P. O. Brown, "Quantitative monitoring of gene expression patterns with a complementary DNA microarray," Science **270**, 467–470 (1995).
[7]M. Schena, D. Shalon, R. Heller, A. Chai, P. O. Brown, and R. W. Davis, "Parallel human genome analysis: Microarray-based expression monitoring of 1000 genes," Proc. Natl. Acad. Sci. U. S. A. **93**, 10614–10619 (1996).
[8]J. Zhang, P. M. Lettinga, J. K. G. Dhont, and E. Stiakakis, "Direct visualization of conformation and dense packing of DNA-based soft colloids," Phys. Rev. Lett. **113**, 268303 (2014).
[9]A. Fallah-Araghi, K. Meguellati, J. C. Baret, A. El Harrak, T. Mangeat, M. Karplus, S. Ladame, C. M. Marques, and A. D. Griffiths, "Enhanced chemical synthesis at soft interfaces: A universal reaction-adsorption mechanism in microcompartments," Phys. Rev. Lett. **112**, 028301 (2014).
[10]A. J. Demello, "Control and detection of chemical reactions in microfluidic systems," Nature **442**, 394–402 (2006).
[11]W. Song, Y. Lavallee, F. B. Wadsworth, K. U. Hess, and D. B. Dingwell, "Wetting and spreading of molten volcanic ash in jet engines," J. Phys. Chem. Lett. **8**, 1878–1884 (2017).
[12]R. D. Deegan, O. Bakajin, T. F. Dupont, G. Huber, S. R. Nagel, and T. A. Witten, "Capillary flow as the cause of ring stains from dried liquid drops," Nature **389**, 827 (1997).
[13]H. Hu and R. G. Larson, "Marangoni effect reverses coffee-ring depositions," J. Phys. Chem. B **110**, 7090–7094 (2006).
[14]H. Kim, F. Boulogne, E. Um, I. Jacobi, E. Button, and H. A. Stone, "Controlled uniform coating from the interplay of Marangoni flows and surface-adsorbed macromolecules," Phys. Rev. Lett. **116**, 124501 (2016).
[15]S. Dash, A. Chandramohan, J. A. Weibel, and S. V. Garimella, "Buoyancy-induced on-the-spot mixing in droplets evaporating on non-wetting surfaces," Phys. Rev. E **90**, 062407 (2014).
[16]L. Pauchard and C. Allain, "Buckling instability induced by polymer solution drying," EPL (Europhys. Lett.) **62**, 897 (2003).
[17]L. Bansal, A. Miglani, and S. Basu, "Universal buckling kinetics in drying nanoparticle-laden droplets on a hydrophobic substrate," Phys. Rev. E **92**, 042304 (2015).
[18]S. Arai and M. Doi, "Anomalous drying dynamics of a polymer solution on a substrate," Eur. Phys. J. E **36**, 63 (2013).
[19]A. L. R. Sibrant and L. Pauchard, "Effect of the particle interactions on the structuration and mechanical strength of particulate materials," EPL (Europhys. Lett.) **116**, 49002 (2016).
[20]L. Bansal, A. Miglani, and S. Basu, "Morphological transitions and buckling characteristics in a nanoparticle-laden sessile droplet resting on a heated hydrophobic substrate," Phys. Rev. E **93**, 042605 (2016).
[21]L. Bansal, S. Basu, and S. Chakraborty, "Confinement suppresses instabilities in particle-laden droplets," Sci. Rep. **7**, 7708 (2017).
[22]L. Pauchard and Y. Couder, "Invagination during the collapse of an inhomogeneous spheroidal shell," EPL (Europhys. Lett.) **66**, 667 (2004).
[23]L. Chen and J. R. Evans, "Drying of colloidal droplets on superhydrophobic surfaces," J. Colloid Interface Sci. **351**, 283–287 (2010).
[24]L. Espín and S. Kumar, "Sagging of evaporating droplets of colloidal suspensions on inclined substrates," Langmuir **30**, 11966–11974 (2014).
[25]L. Espín and S. Kumar, "Forced spreading of films and droplets of colloidal suspensions," J. Fluid Mech. **742**, 495–519 (2014).
[26]W. Y. Ling, T. W. Ng, A. Neild, and Q. Zheng, "Sliding variability of droplets on a hydrophobic incline due to surface entrained air bubbles," J. Colloid Interface Sci. **354**, 832–842 (2011).
[27]S. R. Annapragada, J. Y. Murthy, and S. V. Garimella, "Droplet retention on an incline," Int. J. Heat Mass Transfer **55**, 1457–1465 (2012).
[28]J. Y. Kim, I. G. Hwang, and B. M. Weon, "Evaporation of inclined water droplets," Sci. Rep. **7**, 42848 (2017).
[29]X. Du and R. D. Deegan, "Ring formation on an inclined surface," J. Fluid Mech. **775**, R3-1–R3-12 (2015).
[30]D. Brutin, "Influence of relative humidity and nano-particle concentration on pattern formation and evaporation rate of pinned drying drops of nanofluids," Colloids Surf., A **429**, 112–120 (2013).
[31]S. A. Kulinich and M. Farzaneh, "Effect of contact angle hysteresis on water droplet evaporation from super-hydrophobic surfaces," Appl. Surf. Sci. **255**, 4056–4060 (2009).
[32]N. Anantharaju, M. Panchagnula, and S. Neti, "Evaporating drops on patterned surfaces: Transition from pinned to moving triple line," J. Colloid Interface Sci. **337**, 176–182 (2009).
[33]H. Teisala, M. Tuominen, M. Aromaa, M. Stepien, J. M. Mäkelä, J. J. Saarinen, M. Toivakka, and J. Kuusipalo, "Nanostructures increase water droplet adhesion on hierarchically rough superhydrophobic surfaces," Langmuir **28**, 3138–3145 (2012).
[34]X. Chen, R. Ma, J. Li, C. Hao, W. Guo, B. L. Luk, S. C. Li, S. Yao, and Z. Wang, "Evaporation of droplets on superhydrophobic surfaces: Surface roughness and small droplet size effects," Phys. Rev. Lett. **109**, 116101 (2012).
[35]W. Xu and C. H. Choi, "From sticky to slippery droplets: Dynamics of contact line depinning on superhydrophobic surfaces," Phys. Rev. Lett. **109**, 024504 (2012).
[36]W. Xu, R. Leeladhar, Y. T. Kang, and C. H. Choi, "Evaporation kinetics of sessile water droplets on micropillared superhydrophobic surfaces," Langmuir **29**, 6032–6041 (2013).
[37]A. Bussonnière, M. B. Bigdeli, D. Y. Chueh, Q. Liu, P. Chen, and P. A. Tsai, "Universal wetting transition of an evaporating water droplet on hydrophobic micro-and nano-structures," Soft Matter **13**, 978–984 (2017).
[38]U. U. Ghosh, S. Nair, A. Das, R. Mukherjee, and S. DasGupta, "Replicating and resolving wetting and adhesion characteristics of a rose petal," Colloids Surf., A **561**, 9–17 (2019).
[39]S. Roy, N. Bhandaru, R. Das, G. Harikrishnan, and R. Mukherjee, "Thermally tailored gradient topography surface on elastomeric thin films," ACS Appl. Mater. Interfaces **6**, 6579–6588 (2014).
[40]S. M. Lee, J. Upping, A. Bielawny, and M. Knez, "Structure-based color of natural petals discriminated by polymer replication," ACS Appl. Mater. Interfaces **3**, 30–34 (2011).
[41]B. Bhushan and E. K. Her, "Fabrication of superhydrophobic surfaces with high and low adhesion inspired from rose petal," Langmuir **26**, 8207–8217 (2010).
[42]B. J. Jin and J. Y. Yoo, "Visualization of droplet merging in microchannels using micro-PIV," Exp. Fluids **52**, 235–245 (2012).
[43]L. Bansal, S. Hatte, S. Basu, and S. Chakraborty, "Universal evaporation dynamics of a confined sessile droplet," Appl. Phys. Lett. **111**, 101601 (2017).
[44]L. G. Bremer, P. Walstra, and T. van Vliet, "Estimations of the aggregation time of various colloidal systems," Colloids Surf., A **99**, 121–127 (1995).
[45]A. E. González, F. Martínez-López, A. Moncho-Jordá, and R. Hidalgo-Álvarez, "Two-dimensional colloidal aggregation: Concentration effects," J. Colloid Interface Sci. **246**, 227–234 (2002).
[46]K. H. Kang, S. J. Lee, C. M. Lee, and I. S. Kang, "Quantitative visualization of flow inside an evaporating droplet using the ray tracing method," Meas. Sci. Technol. **15**, 1104 (2004).
[47]J. Xi and L. Jiang, "Biomimic superhydrophobic surface with high adhesive forces," Ind. Eng. Chem. Res. **47**, 6354–6357 (2008).